The change in refractive index of poly(9,9-dioctylfluorene) due to the adoption of the β-phase chain conformation

2007 J. Phys.: Condens. Matter 19 466107

(http://iopscience.iop.org/0953-8984/19/46/466107)

IOP PUBLISHING JOURNAL OF PHYSICS: CONDENSED MATTER

J. Phys.: Condens. Matter **19** (2007) 466107 (14pp) doi:10.1088/0953-8984/19/46/466107

The change in refractive index of poly(9,9-dioctylfluorene) due to the adoption of the β-phase chain conformation

P N Stavrinou, G Ryu, M Campoy-Quiles and D D C Bradley

Experimental Solid State Physics Group, The Blackett Laboratory, Imperial College London, SW7 2AZ, UK

E-mail: p.stavrinou@imperial.ac.uk and d.bradley@imperial.ac.uk

Received 5 July 2007, in final form 4 October 2007
Published 26 October 2007
Online at stacks.iop.org/JPhysCM/19/466107

Abstract

The focus of this work is to study the refractive index in thin films of blue light-emitting poly(9,9-dioctylfluorene) (PFO) that contain extended rigid chains (β-phase). Using a post-deposition exposure to toluene vapour, β-phase chains were induced in glassy PFO films that had been spin coated from a range of solution concentrations to provide thicknesses from 50–200 nm. With the aid of absorption spectroscopy, a semi-empirical calculation of the change in refractive index due to the presence of β-phase chains is undertaken. Over the spectral region where optical gain occurs, the refractive index of β-phase PFO is found to be appreciably larger than for as-spin-coated glassy PFO. Further development and explicit evaluation of the Kramers–Kronig relations lead to analytic and closed form expressions describing the change in index Δn which are used to highlight the key contributions to index change. We find that the spectral response of Δn is largely governed by the emergence of a characteristic absorption band associated with the presence of β-phase chains. The changes in refractive index are experimentally studied by tracking the spectral shifts of optical resonances observed from films spin coated directly onto sub-wavelength 1D grating structures. These measurements are supported and compared with rigorous calculations of the spectra, which incorporate the full optical descriptions for glassy PFO and β-phase PFO. The excellent agreement confirms the accuracy of our semi-empirical extraction approach. Similar polymer-coated grating structures are examined under lasing conditions and can also be used to support the expected spectral response and the decline of Δn for longer wavelengths.

1. Introduction

The blue light emitting polymer poly(9,9-dioctylfluorene) (PFO) has proven to be an interesting material with which to explore the sensitivity of conjugated polymer electronic properties

to variations in physical structure [1–18]. Film samples can be prepared with distinct morphologies via controlled deposition conditions and subsequent thermal and/or vapour treatments, also making use of the fact that PFO is a thermotropic liquid crystal that can be aligned and/or crystallized [1–10]. One can obtain different types of glassy films via spin coating from good solvents and by rapid quenching from the nematic or isotropic melt. Annealing such glassy films or slowly cooling samples from the nematic or isotropic melt leads to crystalline films. Orientation can be achieved on an alignment layer by annealing in the nematic phase and the orientated films can be quenched or crystallized on fast or slow cooling, respectively. Orientated films are of interest for polarized light emission [13], for enhanced charge carrier transport [14, 15] and as a means of enhancing modal gain properties via control over absorption and propagation [19, 20].

A specific extended rigid chain conformation can be obtained in glassy film samples by choice of spin-coating solvent and deposition conditions, by thermal cycling to low temperatures, and by post-deposition exposure to solvent, typically toluene vapour [1–5]. Films that possess a significant fraction of chains with this conformation are termed β-phase samples and they possess characteristically red-shifted absorption and photoluminescence (PL) spectra with well-resolved vibronic features [1–11]. The β-phase samples have a number of interesting photophysical properties and have, for instance, been investigated as systems well suited to the detailed study of energy transfer processes [1–12, 16–18].

While there have been many reports on various aspects of absorption and emission properties of β-phase PFO, until very recently few had considered the resulting index of refraction [21]. That the index of refraction will change is not unexpected—the well known Kramers–Kronig relations relating changes in absorption and refractive index point to this [22]. The question is how large is the change in index? If large enough it can be important in the design of resonator-based structures involving β-phase PFO. Equally important is establishing a reliable technique to probe the index change, particularly given that the fraction of β-phase chains in thin films may be controlled, for example, through the choice of solvent or thermal cycling [3, 5, 7, 9]. The purpose of the present work is to detail a method that reliably extracts the index change arising from the adoption of β-phase chain conformation. Refractive index changes between glassy- and β-phase films are examined, quantified and then verified using resonator-based device environments. Analytic expressions that emerge from the technique are used to highlight the key factors responsible. The overall procedure is quite general and may be used as an accurate way of assessing quite subtle changes in the refractive index of polymer films.

Our approach is based on a semi-empirical calculation of changes in refractive index induced by the conformational changes in β-phase PFO films. These semi-analytic procedures have in the past proved to be very effective for assessing refractive index changes in a number of situations, for example, from electroabsorption in quantum wells [23] and photobleaching in glass waveguides [24]. In investigating the index of refraction for most materials the common starting position usually involves the Kramers–Kronig relations where the refractive index $n(\omega)$ and absorption $\alpha(\omega)$ may be related by [22, 25]

$$n(\omega) = 1 + \frac{c}{\pi}\mathcal{P}\int_0^\infty \frac{\alpha(\omega')}{(\omega')^2 - \omega^2}\,\mathrm{d}\omega', \tag{1}$$

where $\mathcal{P}$ is the principal value. To apply (1) requires knowledge of the absorption over the entire optical spectrum, which in practice is not possible. Instead we make several approximations that allow for more manageable calculations. In the first instance we argue that the refractive index of β-phase PFO films (n_β) can be described in terms of a perturbed glassy-phase refractive index, i.e. $n_\beta = n_\mathrm{g} + \Delta n$ where n_g is the known glassy-phase index

of PFO [26]. Previous studies have estimated that the fraction of the PFO chains that adopt a β-phase conformation in high quality films is typically <20% [5, 7, 8], and in this respect our assumption appears to be a reasonable one. Secondly we assume that all significant changes in absorption are spectrally localized and occur in the vicinity of the main PFO absorption band. The change in refractive index Δn, particularly in the spectral region beyond the main absorption, will be dominated by the local changes in absorption. For energies away from the regions of local absorption change Δn rapidly declines and typically falls-off as $1/\Delta E$, with ΔE the change in photon energy. Thus the integration span for a Kramers–Kronig relation can be restricted to cover only the regions of interest. Explicitly, substituting $n(\omega) = n_g(\omega) + \Delta n(\omega)$ and $\alpha(\omega) = \alpha_g(\omega) + \Delta\alpha(\omega)$ into (1) we find

$$\Delta n(\omega) = \frac{c}{\pi}\mathcal{P}\int_{\omega_a}^{\omega_b} \frac{\Delta\alpha(\omega')}{(\omega')^2 - \omega^2}\,\mathrm{d}\omega', \tag{2}$$

where the localized nature of the problem is now reflected in the integral limits. Results detailing the change in refractive index between glassy- and β-phase PFO films are presented in section 3.1. Following this in section 3.2, analytic expressions are developed to highlight the various contributions and spectral characteristics of the index change, especially around the region where optical gain occurs, i.e. $\lambda \gtrsim 435$ nm.

Turning to the question of how to verify and directly probe the refractive index change, a particularly sensitive approach is to use a shift in the spectral response from a cavity structure, where the material under study constitutes a large part of the cavity. For a given cavity length, any change in the spectral position of the resonance can be attributed to a change in the refractive index, or more specifically the modal *effective* index. For high accuracy, clear visibility of the cavity response is desirable, i.e. the cavity response should have a sufficiently high finesse. To achieve this with a conventional Fabry–Perot resonator would require a film thickness of at least several wavelengths, e.g. for an incident $\lambda \simeq 450$ nm the cavity thickness should be at least 1 μm. However, our desire is to examine the index changes for film thicknesses that are within a range more likely to find application in optical devices (i.e. 100 nm). We turn instead to sub-wavelength patterning to provide the desired optical resonator response and enable the film thicknesses to be kept below <200 nm. A pertinent example of such a structure is a distributed feedback (DFB) resonator, as has been successfully used in many recent investigations of lasing using organic gain media [17, 27–31]. In section 3.3 the spectral shifts from thin films on grating structures, taken from steady state transmission spectra and lasing measurements, are used to probe the index change. The resulting shifts are compared and found to be fully consistent with our refractive index description of β-phase PFO.

2. Experimental section

2.1. Sample preparation

Thin film samples (50–200 nm thickness) of PFO on fused silica (Spectrosil-B) substrates were obtained by spin-coating (1500–5000 rpm) from toluene solutions (5–20 mg ml^{-1}). Toluene is a good solvent for PFO and no β-phase contributions could be observed in the absorption spectra of the as-spin-coated films, which were consistent with a glassy state [1–9]. The β-phase chain conformation was induced by exposing the films to toluene vapour for a period of 12 h at 50 °C. For the experiments involving grating structures, thin films of PFO were spin coated onto fused silica substrates that had 1D gratings etched in the centre; the gratings, which measured 2 mm × 2 mm, were produced by electron-beam lithography and reactive ion

etching. The film thicknesses used for the resonant grating transmission and laser studies were around 200 nm.

2.2. Measurement methods

Absorbance (using a Jasco UV–vis spectrophotometer) and photoluminescence (using a FluoroMax 3 spectrofluorimeter) spectral measurements were routinely taken for each of the samples and used to verify the optical quality of the films.

Film thicknesses were measured with a surface profilometer and used to calculate the absorption coefficients from the measured absorbances. Once converted to absorption coefficient (cm^{-1}) the spectra for the different film thicknesses (50–200 nm) were found to match within 3% in respect of peak heights, confirming that the Beer–Lambert law holds and consequently that (i) the film structure does not change with thickness for these samples and (ii) the absorbance can be used to calibrate film thickness.

Steady-state transmission measurements on the polymer-coated grating structures were performed using a system based on a spectrally filtered white light source with standard lock-in detection techniques. Light from a 150 W xenon lamp, dispersed through a monochromator, is focused onto the sample and the following transmission is collected onto an Si photodiode. A telescopic imaging system was used to monitor the beam position on the sample surface; by imaging the beam on the sample in relation to the grating the spot size was estimated to be around 200 μm. Normal incidence transmission data were recorded with initial spectra taken for films in the as-spin-coated glassy-phase state. After the samples had been subjected to the toluene vapour swelling procedure and the β-phase induced, the measurements were repeated. Two separate measurements were carried out for each sample: one recorded for the monochromatic beam focused onto the grating and one reference measurement in which the focused spot was positioned around 1 mm away from the grating on a planar region of the sample. Normalized transmission spectra were then obtained by dividing the grating spectra by the reference spectra.

For lasing measurements, a 860 μm diameter pump beam, from a frequency trebled Q-switched Nd:YAG laser pumped optical parametric oscillator, was used to deliver 10 ns excitation pulses (10 Hz repetition rate), at 390 nm; the pump beam was incident at an angle of 20° to the plane of the polymer-coated grating. In operation, the emitted lasing light was collected with a fibre bundle, placed normal to the sample surface, and fed to a grating spectrograph equipped with a CCD detector. All measurements were performed at room temperature and in air.

3. Results and discussion

3.1. Extracting the refractive index change from the absorption change

A comparison of the absorption spectra recorded from a thin-film PFO sample, taken first in its glassy-phase and then in its β-phase is shown in figure 1. The glassy-phase spectrum shows the typical broad absorption peak centred around 390 nm while the spectrum recorded for the β-phase film shows the appearance of an additional (characteristic) absorption peak around 435 nm [1–4]. This is perhaps best illustrated in the semi-logarithmic plot in figure 1 (inset), which also helps confirm that, prior to the swelling process, no significant β-phase component is observed. The 435 nm absorption is ascribed to the 0–0 vibronic transition of a β-phase chain segment.

The β-phase and glassy-phase spectra of figure 1 were subtracted to obtain the spectrum of the change of absorption $\Delta\alpha(\omega)$ that is displayed in figure 2 (dotted line). The $\Delta\alpha$ spectrum

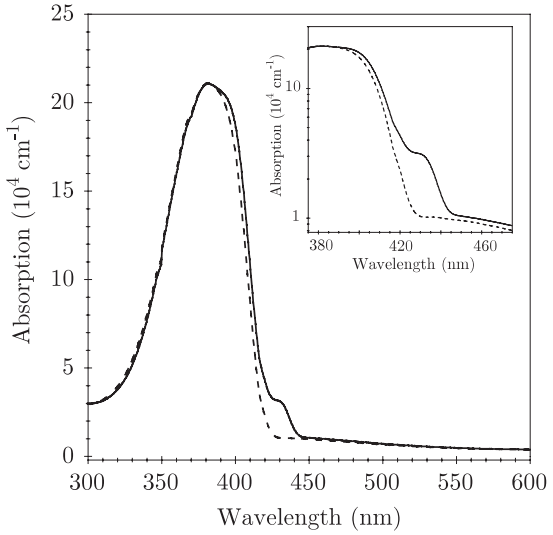

Figure 1. Room temperature absorption spectra of thin films of PFO in the glassy-(dashed line) and β-phase (solid line) state. The inset shows the region around the absorption edge on a semi-logarithmic scale.

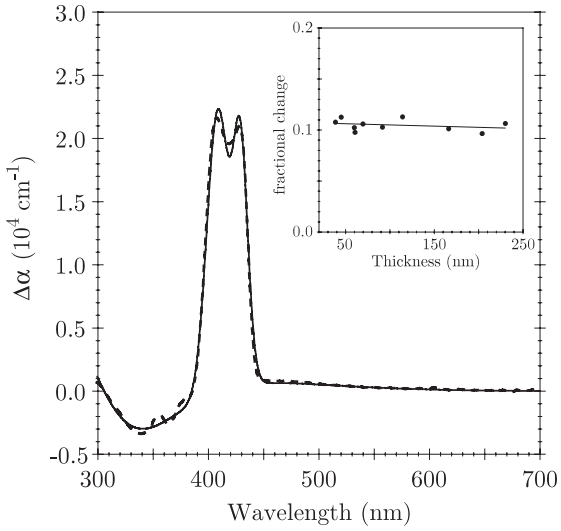

Figure 2. The change in absorption between thin films of PFO and β-phase PFO. Both the experimental (dashed line) and fitted (solid line) spectra are shown. The inset shows the fractional change of absorption around 435 nm (relative to the peak absorption at 390 nm for a number of film thicknesses (see text for details)).

is characterized by three main features: the longest wavelength peak is associated with the β-phase 0–0 absorption peak, the remaining features arise from the other vibronic peaks of the β-phase chain segments and from concomitant changes in the absorption of the non-β-phase segments, some of which convert into the β-phase. Indeed clear vibronic oscillations in the negative part of the $\Delta\alpha$ spectrum are visible for the experimental trace shown in figure 2. The $\Delta\alpha$ spectrum may therefore be viewed as a superposition of a bleaching (negative change) of

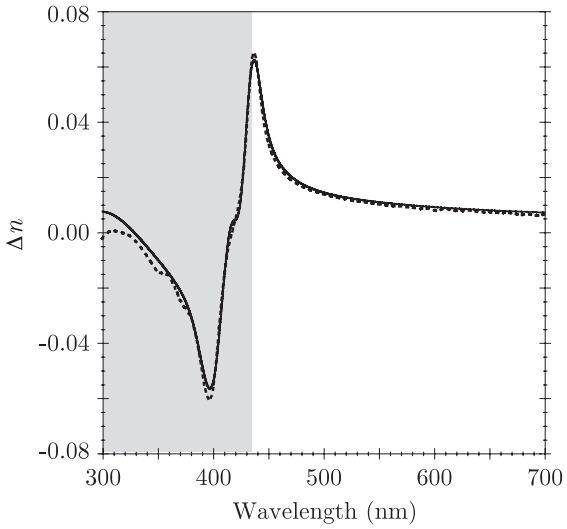

Figure 3. The change in refractive index Δn obtained by numerically evaluating (2) for the experimentally determined $\Delta\alpha$ spectrum (dashed line). The solid line shows Δn obtained from the analytic form given in section 3.2. The shaded region for $\lambda \lesssim 430$ nm indicates the spectral region where significant absorption is present.

the main glassy-phase absorption peak due to conversion of non-β-phase to β-phase segments and the appearance (positive change) of a vibronically structured β-phase absorption. To apply (2) all of these contributions are required; indeed as we show in the following section the higher energy terms, the negative and positive features centred around 330 and 410 nm in figure 2, are a significant contribution to the size of the refractive index change (cf figure 4).

We examined the absorption change spectra from a series of samples, all subjected to the same swelling procedure but prepared from different solution concentrations and consequently of different film thickness. All spectra were remarkably similar and showed the same features identified in figure 2. Once the different thicknesses had been accounted for, we examined the absorption change in the vicinity of the β-phase peak $\Delta\alpha(\lambda_\beta)$ and found values within 10% of each other. These findings are shown in the inset of figure 2 and displayed as a fractional change $\Delta\alpha(\lambda_\beta)/\alpha(\lambda_{\rm pk})$ where $\alpha(\lambda_{\rm pk})$ is the peak value of the β-phase absorption spectra around 390 nm in figure 1. (We note that an equivalent measure may be directly extracted from the UV–vis absorbance measurements on the samples, i.e. $\Delta A(\lambda_\beta)/A(\lambda_{\rm pk})$, and obviates the need for thickness measurements.) The relatively small spread in the fractional change is a useful observation: it verifies that it is possible, for the conditions and thicknesses we have looked at, to induce a certain fraction of β-phase chains. In this respect it is then worthwhile to accurately develop a method to describe the resulting refractive index change. Different β-phase generation procedures, for example changing solvents [7], will produce different fractions of β-phase chains but it should nevertheless be possible to describe the expected changes in index.

Using the absorption change spectra $\Delta\alpha$ in figure 2, numerical integration of (2) was performed and the change in refractive index Δn was obtained. The resulting spectrum is shown in figure 3; for wavelengths longer than the β-phase peak Δn is positive, and decreases rapidly with increasing wavelength. The index change goes to zero around the spectral midpoint of the positive $\Delta\alpha$ region and for shorter wavelengths Δn is negative. Absolute values of Δn reach in excess of 0.06 and represent around a 3% change compared to the glassy-phase PFO

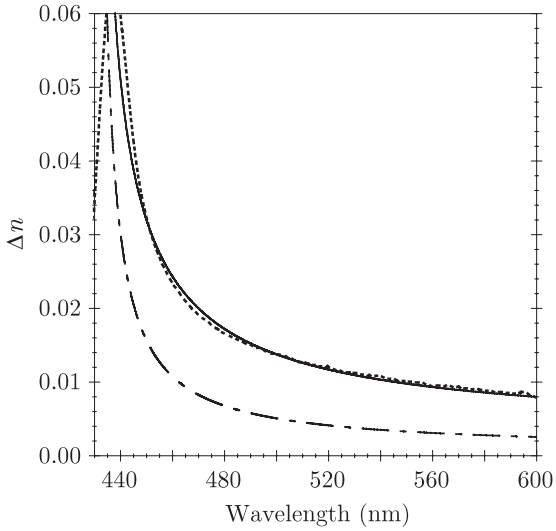

Figure 4. The approximate closed form expression for Δn (solid line) compared to the numerically evaluated Δn (dashed line) obtained from the experimentally determined $\Delta\alpha$ spectrum via (2). Also shown is the contribution to Δn from the 0–0 β-phase absorption peak (dash–dotted line).

index [26]. However, the large absorption present at the wavelengths of maximum Δn means that for the most part the index changes that are accessible to experiments are more modest: in section 3.3, we probe the spectral region beyond the β-phase peak, i.e. $\lambda > 435$ nm where index changes $\Delta n < 2.5\%$ are present. Before doing this we turn towards identifying more clearly the key contributions behind the change in refractive index.

3.2. Analytic and closed form expressions for the refractive index change

To examine the nature and contributions to the change in refractive index we begin with a more general form of the dispersion relation given by (1): that $\widetilde{n}(E) - 1$ is analytic in one half of the complex plane requires the real and imaginary parts to be Hilbert transforms of each other [22, 25]

$$n(E) = 1 + \frac{1}{\pi}\mathcal{P}\int_{-\infty}^{\infty} \frac{\kappa(E')}{E' - E}\,\mathrm{d}E'. \tag{3}$$

Here $n(E)$ and $\kappa(E)$ are the real and imaginary components of the complex refractive index $\widetilde{n}(E)$ and $\mathcal{P}$ denotes the principal value in the Cauchy sense. As in the development from (1) to (2), we consider changes in refractive index Δn and find

$$\Delta n(E) = \frac{1}{\pi}\mathcal{P}\int_{-\infty}^{\infty} \frac{\Delta\kappa(E')}{E' - E}\,\mathrm{d}E'. \tag{4}$$

To make use of (4) the absorption change spectra of figure 2 is converted to represent a change in the extinction coefficient, using $\Delta\kappa(\omega) = c\Delta\alpha(\omega)/(2\omega)$. The resulting spectrum may then be represented using a linear combination of suitable analytic functions; in the present case we use 4 Gaussian functions and write the overall change in extinction spectra as

$$\Delta\kappa(E) = \sum_{j}^{4} \mathcal{L}_j(E), \tag{5}$$

Table 1. The fitting parameters for the 4 Gaussian functions, $\mathcal{L}_j(E)$ in (6), which are used to describe the change in the extinction coefficient.

j	A_j	E_j (eV)	$\sqrt{2}\,\gamma_j$ (eV)
1	0.0588	2.8833	0.0609
2	0.0727	3.0268	0.1075
3	−0.0368	3.7411	0.7200
4	0.0314	3.9654	1.0485

with

$$\mathcal{L}_j(E) = A_j \exp\Big(-\frac{(E-E_j)^2}{2\gamma_j^2}\Big), \tag{6}$$

where an amplitude A_i and linewidth γ^2 characterize each Gaussian function whose values for (5) appear in table 1. The good quality of the fit can be seen in figure 2.

The choice of Gaussian functions for (5) allows the evaluation of the integral on the RHS of (4) to proceed analytically. It is also a reasonable choice given the inhomogeneous broadening that characterizes the spectra of molecular solids. The Hilbert transform of a Gaussian function can be expressed in terms of confluent hypergeometric functions of the first kind ${}_1F_1$ [32–34] and is briefly detailed in the appendix. The change in refractive index (4) may then be written as

$$\Delta n(E) = \sqrt{\frac{2}{\pi}} \sum_j^4 \frac{A_j}{\gamma_j}(E_j - E)\ {}_1F_1\left[1; \frac{3}{2}; -\frac{(E-E_j)^2}{2\gamma_j^2}\right]. \tag{7}$$

Using the parameters listed in table 1 and numerically evaluating (7), the resulting change in refractive index can be compared with that obtained earlier using (2). The full spectral results are shown in figure 3 and they reveal a very good agreement between the two approaches.

Having obtained an analytic form for the index change (7) the salient features responsible for the spectral dependence may be established; of particular interest is the spectral region $\lambda > 435$ nm examined in the following section. We begin with the special functions used in (7) and note they may be expanded [35]

$${}_1F_1\left[1; \tfrac{3}{2}; p\right] = (1/2)(-p)^{-1}\left[1 + \mathrm{O}\left(|p|^{-1}\right)\right],$$

where

$$p = -\frac{(E-E_j)^2}{2\gamma_j^2}.$$

By retaining only the first term in the expansion, the change in refractive index originally described by (7) can be reduced to

$$\Delta n(E) \simeq \sum_j^4 \left(\frac{A_j}{\sqrt{\pi}}\right)\frac{\sqrt{2}\,\gamma_j}{(E_j - E)}. \tag{8}$$

In figure 4 we show Δn the refractive index change predicted from the closed form expression in (8) along with that obtained earlier, from numerically evaluating the experimental absorption change, (2). In the spectral region $\lambda > 435$ nm, the agreement is extremely good; the sharp decline in Δn towards longer wavelengths is clearly evident and, referring to (8), largely follows a $\simeq 1/(\Delta E)$ dependence. Also shown in figure 4 is the contribution to Δn from the β-phase 0–0 vibronic peak, i.e. considering only $j = 1$ in (8). In examining the

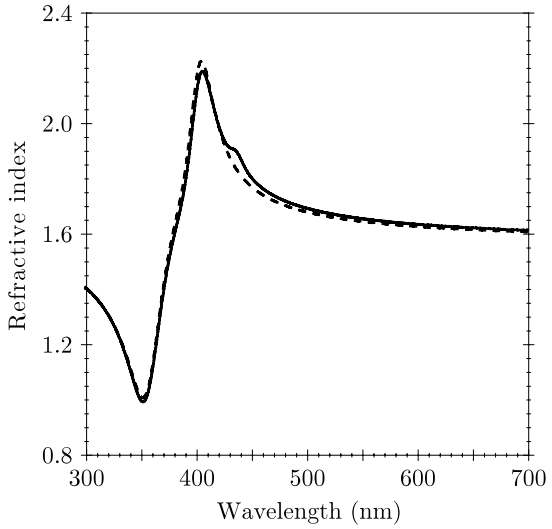

Figure 5. Comparison of the refractive indices for thin films of β-phase PFO (solid line) and glassy PFO (dashed line). The former is obtained from $n_\beta = n_g + \Delta n$ where n_g is the glassy PFO refractive index determined from ellipsometry measurements [26].

spectral dependence in figure 4 the contribution from the β-phase 0–0 vibronic peak appears chiefly responsible for the spectral fall-off in Δn. This alone, however, does not account for the total refractive index change and significant contributions also arise from the other absorption changes. The latter contributions account for over 50% of the total refractive index change and, since the associated transitions occur at higher energies, their contribution to Δn over the spectral region in figure 4 is more or less constant. As noted earlier, these higher energy contributions—the negative and positive peaks in figure 2—are the net effect of the emergence of β-phase chains and the attendant reduction of the main glassy-phase absorption due to conversion of non-β-phase to β-phase segments.

3.3. Measuring the refractive index change

We now turn our attention to direct measurements of the refractive index change induced by the formation of β-phase chain segments and look to verify our predictions for that change. In figure 5 we display the reconstructed refractive index of PFO with β-phase chains present, $n_\beta = n_g + \Delta n$, along with the initial glassy-phase PFO index, n_g. On this scale the change in refractive index is just visible; there is a slight increase in refractive index for the β-phase PFO sample for wavelengths $\gtrsim$ 435 nm. Although the change in index amounts to $\lesssim$ 2%, in this spectral region, it is one for which PFO has a low absorption loss and efficient optical gain [17], making it of interest for photonic applications. With the aid of grating structures, to provide a cavity resonance, we can readily probe these small changes in Δn. We also note that larger changes in absorption can be induced under certain circumstances [2, 3].

The normalized transmission spectra for two samples, with grating periods $\Lambda = 260$ and 290 nm are displayed in figure 6. For each set of spectra, clearly resolved Bragg resonances are visible and appear at 430 nm and 460 nm in figure 6(a) and (b) respectively. Other features seen at 415 nm (figure 6(a)) and 420 nm (figure 6(b)) are artifacts of the normalization procedure and are discussed later. The key result we wish to highlight is the spectral *shift* of the Bragg features, as a result of inducing β-phase chain segments, an effect that is governed by the

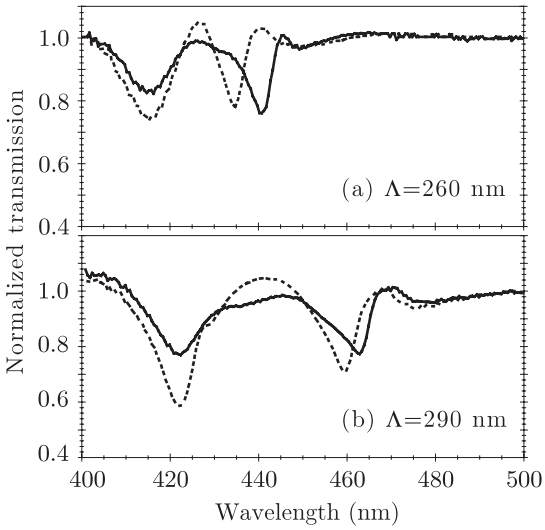

Figure 6. Measured normalized transmission spectra from glassy PFO (dotted line) and β-phase PFO (solid line) thin films sitting atop second order one-dimensional (1D) gratings with period (a) $\Lambda = 260$ nm and (b) $\Lambda = 290$ nm, etched into a quartz substrate.

underlying change in refractive index. The results indicate spectral shifts of around 6 nm and 3 nm for the two samples in figures 6(a) and (b) respectively. As the grating period is increased, the Bragg dip occurs at longer wavelengths and a reduction in the observed shift is observed, which is entirely consistent with the fall-off in Δn shown in figure 4 and described by (8).

These observations can be fully supported by calculating the transmission properties of the structures, which also serves to verify our description of the complex refractive index of β-phase PFO. We use a method based on rigorous coupled wave analysis (RCWA) [36]; our specific implementation has been described in the past [37, 38]. For the calculations, we used the parameters of the structures for which results are shown in figure 6 and the refractive indices for the glassy- and β-phase PFO material are those shown in figure 5, namely $n_{\mathrm{g}}(E)$ and $n_{\beta}(E) = n_{\mathrm{g}}(E) + \Delta n(E)$ with $\Delta n(E)$ obtained from (7).

Figure 7 displays the calculated normalized transmission spectra for the two structures. In comparison with the experimental spectra in figure 6 we find excellent agreement in both the spectral positions of the Bragg resonances and also the spectral shifts. The only fitting parameter used is to allow for a corrugation ($\simeq$30 nm) on the upper surface of the film, shown in the schematic inset figure 7(b). Such corrugations are routinely observed in organic DFB laser studies where the polymer film is spin coated onto a substrate with a grating etched in its surface (see e.g. [39]). Our numerical studies show that surface corrugation has little effect on the spectral position of the longer wavelength Bragg resonance but greatly influences the dip observed at shorter wavelengths (around 415 nm in figure 6(a)). In this spectral region there is a rapid increase in the transmission signal as the main PFO absorption reduces. The appearance of the dip is a result of the normalization of the spectra: we can confirm that no such feature is observed in the raw transmission spectra. While performing our numerical investigations we found that the depth of this dip was reasonably sensitive to the assumed amplitude of the upper surface corrugation, for example only amplitudes between 20 and 40 nm were found to give reasonable agreement with the experimental spectra. This interesting,

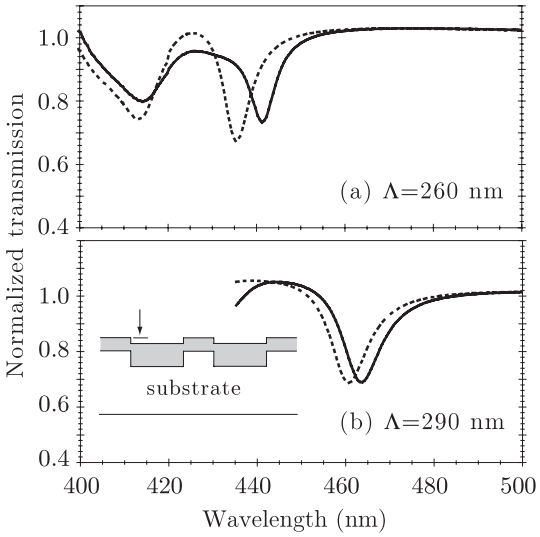

Figure 7. Calculated normalized transmission spectra for structures corresponding to those used to obtain the results shown in figure 6. The inset schematic illustrates the situation where a small thickness corrugation is present at the upper surface of the film.

albeit rather preliminary, observation may suggest a method to optically probe the degree of surface modulation in polymer films on grating structures, although further study should be undertaken[1].

Another approach with which to probe the index change involves taking full advantage of the gain properties of glassy- and β-phase PFO films [17] by monitoring shifts in lasing frequency for second-order DFB structures. Figure 8 shows laser emission from two structures with film thicknesses $\simeq$ 200 nm and grating periods $\Lambda = 260$ and 290 nm. Taking each structure in turn and noting the lasing frequencies for the glassy- and β-phase films, a clear decrease in the red shift of the lasing frequencies (from glassy- to β-phase samples) is observed as the lasing operation is positioned at longer wavelengths (larger period gratings). This is entirely consistent with the trends noted earlier, cf figures 4 and 6, and (8), that Δn decreases with increasing wavelength. We note, however, that in principle the lasing wavelength is also dependent on the distribution of gain, which red shifts as β-phase chain conformations are induced [1, 5, 17]. The resulting shift in lasing wavelength is therefore sensitive to both refractive index changes and optical gain distribution. Nevertheless our preliminary studies here point towards the change in refractive index as the dominant cause of the red shift of the laser wavelength shown in figure 8.

In both of the experimental investigations above we have strictly probed *effective* index changes, Δn_{eff}, due to the wave-guiding nature of the structures studied: the distributed feedback that gives rise to the Bragg resonances occurs in the plane of the films. Such an effective- or modal-index change will have a value less than the true change in material index in figure 4 since the optical mode is distributed over the entire structure, including the lower index substrate and air cladding regions.

[1] We have used a simple square grating for the upper surface corrugation for the present calculations. In practice the surface grating profile is more likely to have a sinusoidal profile, as indeed suggested by our own AFM studies on a number of laser structures. A more detailed study is planned.

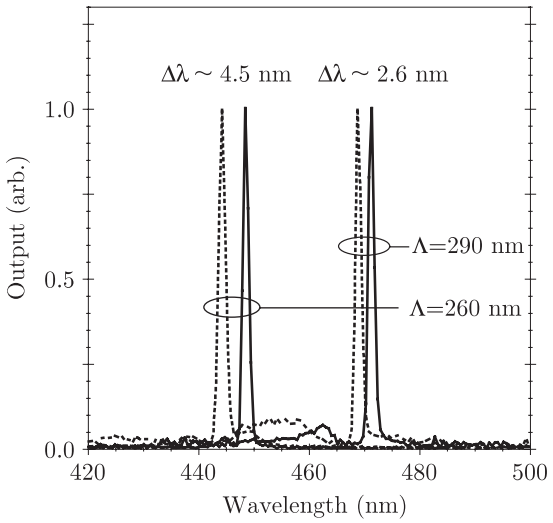

Figure 8. Lasing emission from glassy-phase (dotted) and β-phase (solid) PFO films spin coated onto second order 1D gratings (a) $\Lambda = 260$ nm, (b) $\Lambda = 290$ nm.

4. Conclusion

We have presented a detailed study of the refractive index properties of PFO films that possess a fraction of chains with extended, planar β-phase conformation. For our work the β-phase conformation was induced using a post-deposition exposure to toluene vapour. By monitoring the change in absorption spectra, the fraction of β-phase chains induced for a range of film thicknesses and concentrations was found to be approximately the same. A Kramers–Kronig analysis was used to extract the change in the index of refraction for β-phase films in comparison with spin-coated glassy films. Analytic and closed form expressions were developed and used to shed greater light on the relative contributions to the index change. The β-phase 0–0 vibronic peak, around 435 nm, was found to be chiefly responsible for the spectral dependence and accounted for just under 50% of the total index change Δn in the visible wavelength range. Over the spectral region where optical gain occurs, the increase in refractive index was found to be between 1–2% for the samples studied here. Several additional optical experiments were performed to check the changes in Δn: transmission spectra were recorded for second order DFB structures and the observed spectral shifts in the Bragg resonances were described in terms of an underlying increase in the refractive index for films containing β-phase chains. The size of the red shift was found to rapidly decrease as the resonance was spectrally positioned further away from the β-phase 0–0 vibronic absorption peak, which is fully consistent with our expectations. Furthermore, simulations of the spectral response and resonance shifts, using the extracted optical properties of β-phase PFO, were found to give excellent agreement with measurements. Similar observations were found when the structures were examined under lasing operation. It is hoped that the study will have highlighted the utility and consistency of a semi-empirical Kramers–Kronig approach which might now be applied to probe the optical response due to conformation changes in a number of polymeric systems.

Acknowledgments

The authors would like to thank Ruidong Xia, Colin Belton and Xuhua Wang for useful discussions. We also thank Sumitomo Chemical Co. Ltd for providing the polyfluorene used

for this study. This work was supported by the United Kingdom Engineering and Physical Sciences Research Council (EPSRC): GR/R55078 Ultrafast Photonics Collaboration IRC and EP/C539494 Advanced Research Fellowship Award (PNS).

Appendix

The Hilbert transform of a function is often defined by [22, 25, 32]

$$(\mathcal{H}f)(x) = \frac{1}{\pi}\mathcal{P}\int_{-\infty}^{\infty}\frac{f(x')}{x'-x}\,\mathrm{d}x', \tag{A.1}$$

where $\mathcal{P}$ denotes the Cauchy principal value. Our interest lies with the case where $f(x)$ is square integrable and defined on the real line, $f(x) \in L_2(-\infty, \infty)$, and following (A.1) the resulting function shares the same properties. It is worth noting that some authors [32] define the forward transform in an opposite sign convention to that shown in (A.1) and consequently the resulting transforms will differ from ours by a factor of (-1). We consider a Gaussian function $f(x) = \exp(-a^2(x-b)^2)$ where a and b are constants. The Hilbert transform of the Gaussian can be developed as follows,

$$\begin{aligned} H\left[f(x)\right] &= \mathrm{i}\mathrm{e}^{-a^2(x-b)^2}\operatorname{erf}\left(\mathrm{i}a(x-b)\right) \\ &= -2\frac{a(x-b)}{\sqrt{\pi}}\mathrm{e}^{-a^2(x-b)^2}\,{}_1F_1\left[\frac{1}{2};\frac{3}{2};a^2(x-b)^2\right] \\ &= 2\frac{a(b-x)}{\sqrt{\pi}}\,{}_1F_1\left[1;\frac{3}{2};-a^2(x-b)^2\right]. \end{aligned} \tag{A.2}$$

To arrive at the final line of (A.2) we have made use of the following identities [35],

$$\begin{aligned} &\operatorname{erf}(\mathrm{i}z) = \mathrm{i}\frac{2}{\sqrt{\pi}}z\,{}_1F_1\left[\frac{1}{2};\frac{3}{2};z^2\right] \\ &{}_1F_1\left[\frac{1}{2};\frac{3}{2};z^2\right] = \mathrm{e}^{z^2}\,{}_1F_1\left[1;\frac{3}{2};-z^2\right]. \end{aligned} \tag{A.3}$$

The numerical studies in section 3.2 made use of the following integral representation,

$${}_1F_1\left[1;\frac{3}{2};-z^2\right] = \frac{1}{2}\int_0^1 \mathrm{e}^{-z^2t}(1-t)^{-\frac{1}{2}}\,\mathrm{d}t. \tag{A.4}$$

Finally we note the Hilbert transform of a Gaussian can be expressed using other special functions [40], such as the Dawson function $D(z)$. The connection between this approach and (A.2) is straightforward given the close relationship between $D(z)$ and the error function, $D(z) = -\mathrm{i}(\sqrt{\pi}/2)\mathrm{e}^{-z^2}\operatorname{erf}(\mathrm{i}z)$. Indeed formulating the problem in terms of $D(z)$ and using the property that for large z, $D(z) \approx (2z)^{-1}$ we arrive at the same dependence for the index change (8) presented at the end of section 3.2.

References

[1] Grell M, Bradley D D C, Inbasekaran M and Woo E P 1997 *Adv. Mater.* **9** 798
[2] Grell M, Bradley D D C, Long X, Chamberlain T, Inbasekaran M, Woo E P and Soliman M 1998 *Acta Polym.* **49** 439
[3] Grell M, Bradley D D C, Ungar G, Hill J and Whitehead K S 1999 *Macromolecules* **32** 5810
[4] Cadby A J, Lane P A, Mellor H, Martin S J, Grell M, Giebeler C, Bradley D D C, Wohlgenannt M, An C and Vardeny Z V 2000 *Phys. Rev.* B **62** 15604
[5] Ariu M, Sims M, Rahn M D, Hill J, Fox A M, Lidzey D G, Oda M, Cabanillas-Gonzalez J and Bradley D D C 2003 *Phys. Rev.* B **67** 195333

[6] Sims M, Zheng K, Campoy-Quiles M, Xia R, Stavrinou P N, Bradley D D C and Etchegoin P 2005 *J. Phys.: Condens. Matter* **14** 6307
[7] Kahn A L T, Sreearunothai P, Herz L M, Banach M J and Köhler A 2004 *Phys. Rev.* B **69** 085201
[8] Hayer A, Kahn A L T, Friend R H and Köhler A 2005 *Phys. Rev.* B **71** 241302(R)
[9] Winokur M J, Slinker J and Huber D L 2003 *Phys. Rev.* B **67** 184106
[10] Chunwaschirasiri W, Tanto B, Huber D L and Winokur M J 2005 *Phys. Rev. Lett.* **94** 107402
[11] Korovyanko O J and Vardeny Z V 2002 *Chem. Phys. Lett.* **356** 361
[12] Rothe C, King S M, Dias F and Monkman A P 2004 *Phys. Rev.* B **70** 195213
[13] Whitehead K S, Grell M, Bradley D D C, Jandke M and Strohriegl P 2000 *Appl. Phys. Lett.* **76** 2946
[14] Redecker M, Bradley D D C, Inbasekaran M and Woo E P 1998 *Appl. Phys. Lett.* **73** 1565
[15] Kreouzis T, Poplavskyy D, Tuladhar S M, Campoy-Quiles M, Nelson J and Bradley D D C 2006 *Phys. Rev.* B **73** 235201
[16] Virgili T, Marinotto D, Lanzani G and Bradley D D C 2005 *Appl. Phys. Lett.* **86** 091113
[17] Ryu G, Xia R and Bradley D D C 2007 *J. Phys.: Condens. Matter* **19** 056205
[18] Rothe C, Galbrecht F, Scherf U and Monkman A P 2006 *Adv. Mater.* **18** 2137
[19] Heliotis G, Xia R, Whitehead K S, Turnbull G A, Samuel I D W and Bradley D D C 2003 *Synth. Met.* **139** 727
[20] Xia R, Campoy-Quiles M, Heliotis G, Stavrinou P N, Whitehead K S and Bradley D D C 2005 *Synth. Met.* **155** 274
[21] Azuma H, Kobayashi T, Shim Y, Mamedov N and Naito H 2007 *Org. Electron.* **8** 184
[22] Nussenzveig H M 1972 *Causality and Dispersion Relations* 2nd edn (New York: Academic)
[23] Weiner J S, Miller D A B and Chemla D S 1987 *Appl. Phys. Lett.* **50** 842
[24] Roman J E and Winick K A 1993 *Opt. Lett.* **18** 808
[25] Peiponen K E and Vartiainen E M 1991 *Phys. Rev.* B **44** 8301
[26] Campoy-Quiles M, Heliotis G, Xia R, Ariu M, Pantani M, Etchegoin P G and Bradley D D C 2005 *Adv. Funct. Mater.* **15** 925
[27] McGhehee M D, Diaz-Garcia M A, Hide F, Gupta R, Miller E K and Moses D 1998 *Appl. Phys. Lett.* **72** 1536
[28] Heliotis G, Xia R, Bradley D D C, Turnbull G A, Samuel I D W, Andrew P and Barnes W L 2003 *Appl. Phys. Lett.* **83** 2118
[29] Heliotis G, Xia R, Turnbull G A, Andrew P, Barnes W L, Samuel I D W and Bradley D D C 2004 *Adv. Funct. Mater.* **14** 91
[30] Xia R, Heliotis G, Stavrinou P N and Bradley D D C 2005 *Appl. Phys. Lett.* **87** 031104
[31] Heliotis G, Choulis S A, Itskos G, Xia R, Murray R, Stavrinou P N and Bradley D D C 2006 *Appl. Phys. Lett.* **88** 081104
[32] King F W 2002 *J. Opt. Soc. Am.* B **19** 2427
[33] Kim J, Lerttamrab M, Chuang S L, Gmachl C, Sivco D L, Capasso F and Cho A Y 2004 *IEEE J. Quantum Electron.* **40** 1663
[34] Kim J and Chuang S-L 2006 *IEEE J. Quantum Electron.* **42** 942–52
[35] Abramowitz M and Stegun I 1972 *Handbook of Mathematical Functions* 9th edn (New York: Dover)
[36] Moharam M G, Grann E B, Pommet D A and Gaylord T K 1995 *J. Opt. Soc. Am.* A **12** 1068
[37] Stavrinou P N and Solymar L 2002 *Opt. Commun.* **206** 217
[38] Stavrinou P N and Solymar L 2003 *Phys. Rev.* E **68** 066604
[39] Turnbull G A, Andrew P, Jory M J, Barnes W L and Samuel I D W 2001 *Phys. Rev.* B **64** 125122
[40] Weideman J A C 1995 *Math. Comput.* **64** 745